CONTROL VOLUME METHOD FOR THE DYNAMO PROBLEM IN THE SPHERE WITH THE FREE ROTATING INNER CORE

P. HEJDA[1] AND M. RESHETNYAK[2,3]

1 Geophysical Institute, Acad. Sci. Czech Republic, Boční II/1401, 141 31 Prague 4, Czech Republic (ph@ig.cas.cz)
2 Institute of the Physics of the Earth, Russian Acad. Sci., Bolshaya Gruzinskaya 10, 123995 Moscow, Russia (maxim@uipe-ras.scgis.ru)
3 Research Computing Center of Moscow State University, 119899, Moscow, Russia

Received: April 5, 2002; Accepted: October 22, 2002

ABSTRACT

A model of thermally driven dynamo in the Boussinesq approximation in the spherical shell with the free rotating inner core is considered. To solve equations we use a new in dynamo modeling control volume technique (for details of this method for hydrodynamics see Patankar, 1980). The main advantage of this method over previous attempts to solve magnetohydrodynamics equations in the spherical grids is that no filtering of high harmonics in the pole regions is needed. We present the results of simulations for the self-consistent dynamo system evolution over the diffusion time and longer periods. Different ways of stabilizations of magnetohydrodynamics equations, when convective terms are of the same order (or larger) as conductive ones, are considered.

Keywords: hydromagnetic dynamo, finite volumes, SIMPLE algorithm, up-wind scheme

1. INTRODUCTION

The last decade revealed a dramatic progress in dynamo modeling (*Jones, 2000*). Many new models of self-consistent dynamo based on the thermal convection for compressible and non-compressible conducting fluid (*Glatzmaier and Roberts, 1995a; Kuang and Bloxham, 1997*), compositional convection (*Glatzmaier and Roberts, 1996*), including sometimes equations of thermodynamical state (*Kageyama et al., 1993*) were developed. In contrast to the variety of these models nearly all of them are based on a similar numerical approach which dates back to the pioneering work of *Bullard and Gellman (1954)*. It consists of decomposition of the magnetic and velocity fields into toroidal and poloidal potentials and expansion of these functions into spherical functions (spectral method). As regards radial dependence some polynomials, like, e.g., Chebyshev or finite differences, are used (see the overview of the numerical methods used in the dynamo models in *Christensen et al., 2001*). These specifics of the dynamo modeling originate in the theoretical bases of the dynamo theory and the special (spherical) geometry of the problem.

Nevertheless, there were also attempts to solve the dynamo equations by using grid methods. Among the first such works was the well known Braginsky's *Z*-model (*Braginsky, 1976; Braginsky and Roberts, 1987*), where the full grid method was combined with the toroidal-poloidal decomposition of 2D magnetic and velocity fields. The main advantage of the full grid approach is the comparative simplicity of discretization. In spite of the fact that the last comparison of the different set of dynamo models, which used fully spectral methods or combination of spectral methods and grids, showed that the pure spectral methods were more accurate for the more or less smooth 3D dynamo solutions (*Christensen et al., 2001*), this advantage can disappear when discretization of small irregular structures is required. This phenomenon was shown by *Anufriev et al. (1995)* in the study of 2D dynamo models for low Ekman numbers.

A natural way to extend the 2D grid method to the solution of 3D models is to expand the φ-variable into Fourier series. As the grid methods were successfully developed and applied to the solution of a broad class of 2D models (e.g. *Anufriev and Hejda, 1998a,*b), it could be expected that such generalization would not bring any essential problems. Nevertheless, the opposite is the truth. One crucial problem is that in the full 3D model all harmonics have to be resolved up to $m \approx E^{-1/3}$ (*Roberts, 1968*) (where E is the Ekman number, see below). The second problem is the stability of the finite-difference methods near the axis. *Gilman and Miller (1981)* already solved Sun-like dynamo models in a spherical shell and revealed the problem of stability of the solution in the polar regions. To prevent computational instabilities they either used a perfectly conducting and thermal insulating wall at the latitude of 75°N and S or used rather crude filtering of higher Fourier harmonics in the polar regions. Similar filtering techniques were also applied by *Kageyama et al. (1993)* in their method based on the second-order finite differencing in all directions. It is obvious that those simplifications are beyond the usual limit acceptable in dynamo modeling.

Using exact asymptotics, which follows from the basic properties of the vector fields near the axis of the rotation, the problem can be overcome (*Nakajima and Roberts, 1995; Hejda and Reshetnyak, 2000; Hejda et al., 2001*). Nevertheless, the applicability of the method is limited due to its intrinsic instability even in the case of pure convection.

The grounds of difficulties in solving magnetohydrodynamics (MHD) equations on regular grids in spherical coordinates are well known. There are singularities of the equations on the axis of rotation on the one hand and restriction on the time step, caused by the closeness of the longitudinal grid points near the axis of rotation, on the other hand. One of the ways to overcome these problems is to rewrite all equations at the axis points using different system of coordinates, e.g., the Cartesian, where equations are regular (*Rädler, personal communication, 2000*). However, the problem in the other points in the vicinity of the axis still exists and additional numerical tricks must be applied.

In the present work we introduce a different approach, in which the difficulties caused by singularities of the coefficients were solved by using the weighted coefficients (the control volumes). The basic strategy of this numerical scheme, otherwise known as the finite volume method, is to write the differential equations at each point in the conservative form, to integrate them over the control volume (with the centre in this point) and convert each such integral into sum of integrals over the boundary faces by means of Gauss theorem. As the area of the faces close to the axis of rotation is indirectly

proportional to the singular coefficients, the resulting grid equations are non-singular. The control volume formulation of the problem allows utilizing a whole range of techniques which were developed in hydrodynamics (see e.g., *Fletcher, 1988; Patankar, 1980*) or even in MHD simulations (*Evans and Hawley, 1988*) for the stabilization of convective terms (e.g., up-wind schemes).

In this paper we describe the development of the control volume method (*Pantakar, 1980*) for the 3D thermally driven dynamo in Boussinesq approximation in the sphere. Different schemes of convective terms approximations are considered. This approach demonstrates very stable behavior of the fields and no problems appear near the axis. Some solutions of the fully 3D dynamo simulations with the free rotating inner core are presented.

2. BASIC EQUATIONS

The dynamo process driven by the flows of incompressible fluid ($\nabla \cdot \boldsymbol{V} = 0$) in the Boussinesq approximation in the spherical shell ($r_i < r < r_0$) rotating with the angular velocity Ω is described by the induction equation

$$\frac{\partial \boldsymbol{B}}{\partial t} = \nabla \times (\boldsymbol{V} \times \boldsymbol{B}) + \nabla^2 \boldsymbol{B}\,, \tag{2.1}$$

the Navier-Stokes equation

$$R_o\left(\frac{\partial \boldsymbol{V}}{\partial t} + (\boldsymbol{V} \cdot \nabla)\boldsymbol{V}\right) = -\nabla P + \boldsymbol{F} + E\nabla^2 \boldsymbol{V} \tag{2.2}$$

and the heat flux equation

$$\frac{\partial T}{\partial t} + \boldsymbol{V} \cdot \nabla (T + T_o) = q\nabla^2 T\,. \tag{2.3}$$

The equations are scaled with the radius of the sphere L as the fundamental length scale, which makes the dimensionless radius $r_o = 1$; the inner core radius r_i is, similarly to the one of the Earth, equal to 0.35.

Velocity $\boldsymbol{V}$, magnetic field $\boldsymbol{B}$, pressure P and time t are measured in units of η/L, $\sqrt{2\Omega\eta\mu\rho}$, $\rho\eta^2/L^2$ and L^2/η, respectively, where η is magnetic diffusivity, ρ is density, μ permeability, $R_o = \eta/2\Omega L^2$ is the Rossby number, $E = \nu/2\Omega L^2$ is the Ekman number, ν is kinematic viscosity. T is the temperature deviation from the prescribed temperature profile $T_0 = \dfrac{r_i/(r-1)}{1-r_i}$ (*Tilgner and Busse, 1997*). The force F includes the Coriolis, Archimedean and Lorentz effects:

$$\boldsymbol{F} = -\boldsymbol{1}_z \times \boldsymbol{V} + qR_a Tr\boldsymbol{1}_r + (\nabla \times \boldsymbol{B}) \times \boldsymbol{B}\,, \tag{2.4}$$

where (r,θ,φ) is the spherical coordinate system, $\boldsymbol{1}_z$ is the unit vector along the axis of rotation and $R_a = \alpha g_o \delta T L/2\Omega\kappa$ is the modified Rayleigh number, α is the coefficient of

volume expansion, δT is the drop of temperature through the shell, g_o is the gravity acceleration at $r = r_0$ and $q = \kappa/\eta$ is the Roberts number.

In general, the inner core ($r \le r_i$) can rotate around axis z due to the viscous and magnetic torques τ. The momentum equation for the angular velocity ω of the inner core has the form:

$$R_o I \frac{\partial \omega}{\partial t} = r_i \oint_S \tau_{r\varphi}\Big|_{r=r_i} \sin\theta \, dS \,, \tag{2.5}$$

where I is the moment of inertia of the inner core, S is the surface of the core and the stress tensor components are defined as $\tau_{r\varphi} = E\left(\frac{\partial V_\varphi}{\partial r} + \frac{1}{r\sin\theta}\frac{\partial V_r}{\partial \varphi} - \frac{V_\varphi}{r} \right) + B_r B_\varphi \sin\theta$.

Eqs(2.1–2.5) are closed by the non-penetrating and no-slip boundary conditions for the velocity field at the rigid surfaces and zero boundary conditions for temperature perturbations. Vacuum boundary conditions were used for the magnetic field at $r = r_0$. So far the magnetic diffusivity of the inner core was the same as for the outer one and we do not consider current layers at the core-mantle boundary, the magnetic field is continuous at the boundary.

3. NUMERICAL METHODS

To solve MHD equations (2.1–2.3) we have used the control volume method described in detail for thermal hydrodynamics (without the magnetic field) for Cartesian geometry in (*Patankar, 1980*). It is assumed that all fields are defined in the nodes which are the centers of the staggered grid cells (control volumes). The basic strategy of the method is to express the differential equations in conservative form, integrate them over the control volumes and convert every such integral into the sum of fluxes over the boundary faces by means of Gauss' theorem. It is advantageous to employ a different grid for each component of vector fields (and an additional grid for the scalar field). Then, if we consider the heat flux equation, the velocity components are calculated for the points that lie on the corresponding faces of the control volumes (v_r is calculated at the faces that are normal to the r-direction, etc.).

To be more definite, let us consider control volume $\mathcal{V}$ with central point P, which has grid points E and W as its neighbors in the r-direction, N and S in the θ-direction and T, and B in the φ-direction (see Fig. 1). Small letters denote the corresponding faces, the symbol $\mathcal{F}$ its area and δ the distance between point P and its neighbors. For example,

$$\mathcal{F}_e = r_e^2 \sin\theta_P (\theta_n - \theta_s)(\varphi_t - \varphi_b), \; \delta_e = r_E - r_P \,,$$

$$\mathcal{F}_n = r_P \sin\theta_n (r_e - r_w)(\varphi_t - \varphi_b), \; \delta_n = r_P(\theta_N - \theta_P),$$

$$\mathcal{F}_t = r_P (r_e - r_w)(\theta_n - \theta_s), \; \delta_t = r_P \sin\theta_P (\varphi_T - \varphi_P) \,.$$

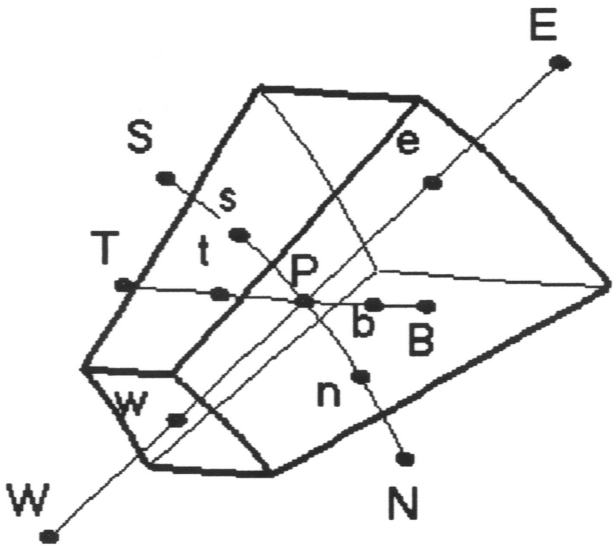

Fig. 1. Control volume in the spherical grid.

Integrating the equation over control volume $\mathcal{V}$ and using Gauss' theorem, we get the following approximation:

$$\int_{\mathcal{V}} q\nabla^2 T dV \approx D_e T_E + D_w T_W + D_n T_N + D_s T_S + D_t T_T + D_b T_B - D_P T_P , \tag{3.1}$$

where $D_P = D_e + D_w + D_n + D_s + D_t + D_b$, $D_e = q\,\mathcal{F}_e/\delta_e$ and similarly for *w*, *n*, *s*, *t*, *b*,

$$\begin{aligned} \int_{\mathcal{V}} \boldsymbol{V}\cdot\nabla T\, dV &= \int_{\mathcal{V}} \nabla\cdot(T\boldsymbol{V})\, dV \\ &\approx \frac{1}{2}\left(F_e T_E - F_w T_W + F_n T_N - F_s T_S + F_t T_T - F_b T_B\right), \end{aligned} \tag{3.2}$$

where $F_e = (V_r)_e \mathcal{F}_e$, $F_n = (V_\theta)_n \mathcal{F}_n$, and so on. The temperature at the interface was put equal to the average at neighboring points (e.g. $T_e = (T_P + T_E)/2$). We have also used the fact that $F_e - F_w + F_n - F_s + F_t - F_b = 0$, which follows from the equation of continuity.

As we are using the fully implicit scheme, the first term in (2.3) can be approximated by

$$\int_{\mathcal{V}} \frac{\partial T}{\partial t} dV \approx \left(T_P - T_P^o\right)\frac{W}{\Delta t} \tag{3.3}$$

where W is the volume of $\mathcal{V}$, Δt the length of the time step and index "o" denotes the value at the previous time step.

The heat flux equation can thus be expressed as

$$\left(a_P + \frac{W}{\Delta t}\right) T_p = a_E T_E + a_W T_W + a_N T_N + a_S T_S + a_B T_B + a_T T_T + b\,, \tag{3.4}$$

where

$$a_E = D_e - \frac{F_e}{2},\ a_N = D_n - \frac{F_n}{2},\ a_T = D_t - \frac{F_t}{2}$$

$$a_W = D_w + \frac{F_w}{2},\ a_S = D_s + \frac{F_s}{2},\ a_B = D_b + \frac{F_b}{2}$$

$$a_P = a_E + a_W + a_N + a_S + a_T + a_B$$

and

$$b = \frac{W T_P^o}{\Delta t} + \text{ approximation of } \int_{\mathcal{V}} \boldsymbol{V} \cdot \nabla T_o \; dV$$

The system of equations (3.4) has a block tridiagonal structure and must be solved by an iterative method (e.g., Gauss-Seidel). Direct solution of the inner-most tridiagonal blocks speeds up the solution.

Unless the Reynolds number is small enough, some of the coefficients a_* can be negative. This will violate the condition of diagonal dominance of the resulting matrix and either cause failure of the iteration process, or lead to an unrealistic solution. A well-known remedy for this difficulty is the up-wind scheme. It recognizes that the weak point of the above formulation is the approximation of T at the interface by the average of the neighboring grid points and suggests putting it equal to the value at the up-wind side of the face. For example

$$T_e = T_P \text{ if } F_e > 0,\ T_e = T_E \text{ if } F_e < 0\,. \tag{3.5}$$

Details of the numeric implementation of the up-wind scheme, as well as similar techniques (power-law or hybrid schemes) can be found in (*Patankar, 1980*).

The other equations for the vector components of $\boldsymbol{V}$ and $\boldsymbol{B}$ are discretized in a similar way. In the case of the magnetic field equations, the convective terms were considered implicitly. In the Navier-Stokes equation we considered the non-linear term in linearized form $\left(\boldsymbol{V}_{n+1}^{m} \cdot \nabla\right)\boldsymbol{V}_{n+1}^{m+1}$, where n is the time step, and m is the current number of iteration in the Gauss-Seidel algorithm. The Lorentz force in the Navier-Stokes equation is an "external" source and is approximated by central differences. To find the B_r-component of the magnetic field we have used the equation of continuity $\nabla \cdot \boldsymbol{B} = 0$.

All equations were iterated until the following conditions for every elementary control volume were satisfied: a) the condition of continuity for the velocity field; b) the conservation law for the fluxes in the heat-flux equation; c) the stable state for the magnetic field. The magnitude of the time step was chosen in such a way that the number of these iterations was about ten. After that a new time step started.

In many cases the control volume technique provides an easy way of omitting the boundary condition at the axis (or in the center of coordinates). This follows from the fact that the size of the face of the elementary control volume at the axis (and in the center) is zero. (Note also, that when the axis (center) is approached, the size of the current control volume decreases). If, during the solution for one component, the value of the other component at the axis (center) is needed, we use extrapolation (see also *Kageyama et al.,*

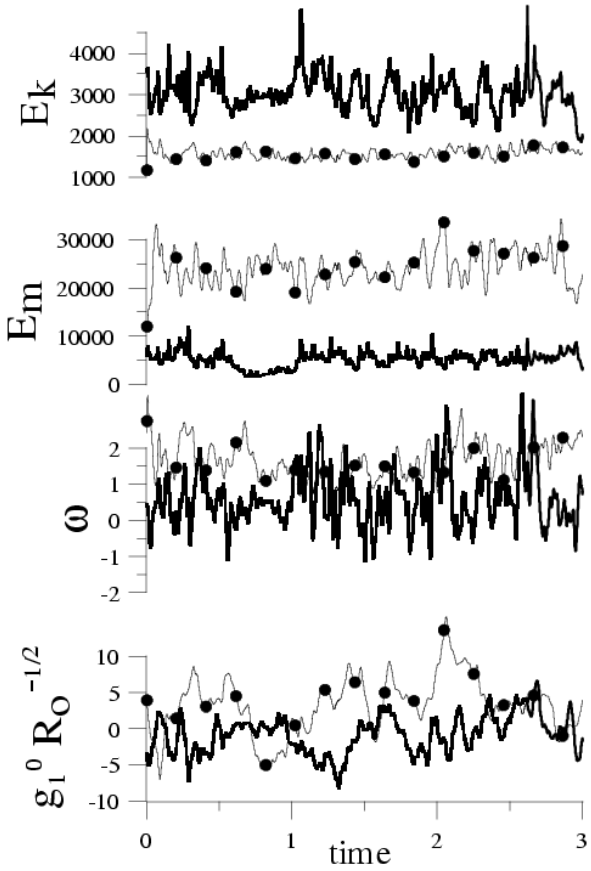

Fig. 2. Evolution of (from top to bottom) the kinetic energy, magnetic energy, angular velocity of the inner core and normalized dipole coefficient for two regimes: case I (thick line) – $E = R_o = 10^{-1}$, $R_a = 3 \times 10^3$ and $q = 3$; case II (circles) – $E = 10^{-2}$, $R_o = 10^{-3}$, $R_a = 500$ and $q = 1$.

1993). For all scalar quantities and r-components of the vectors we apply condition $\frac{\partial}{\partial\theta} = 0$ by using only the axisymmetrical part of the fields obtained by the Fourier decomposition for the two adjacent in the θ-layers near the axis and by extrapolating. The same extrapolation is used for the θ- and φ-vector components of the field, but for the $m = 1$ mode in the Fourier series.

The details of the vacuum boundary conditions for the magnetic field are described in *Hejda and Reshetnyak (2000)*. (Here we used 8 spherical functions.) As follows from testing the program similar to that in *Hejda and Reshetnyak (2000)*, the magnetic field in the center requires special treatment. For this aim we used asymptotics derived from the free decay modes for the 2nd and 3rd layers near the center.

4. RESULTS OF SIMULATIONS

The test computations were done on a simple Pentium-III processor. For the given parameters we first calculated the thermal convection without a magnetic field and after that the entire set of equations was integrated, starting from the initial seed of the magnetic field given by the arbitrary free decay mode solution. The integration over a time interval of several units (in a dimensionless system of units) was carried out in order to exclude solutions in which the magnetic field grows initially but then it dies out. This procedure is very time consuming and, therefore, a great part of the computations was carried out on a coarse grid $(r,\theta,\varphi) = (16,16,16)$. The mesh size imposes limitations on the range of parameters. It is, for example, well known (*Roberts, 1968*) that the space scale $l \approx E^{1/3}$. Although we were not able to carry out long-term computations on finer grids, several short-term computations confirmed the high stability of the developed computer code.

To analyze the mean characteristics of the model, we evaluated the kinetic and magnetic energies of the system,

$$E_k = \frac{1}{2}\int \boldsymbol{V}^2 \, d\boldsymbol{r}^3 \,, \quad E_m = \frac{1}{2R_o}\int B^2 \, d\boldsymbol{r}^3 \,, \tag{4.1}$$

where velocity is integrated over the shell and the magnetic field over the full sphere. This normalization of the magnetic energy follows from the non-dimensional form of equations (2.1–2.2). We also introduce normalization of the first axi-symmetrical Gauss coefficient g_1^0 using factor $R_o^{-1/2}$. The upper two plots in Fig. 2 demonstrate the evolution of kinetic and magnetic energies over three diffusion times for two regimes: $E = R_o = 10^{-1}$, $R_a = 3 \times 10^3$, $q = 3$ (regime I) and $E = 10^{-2}$, $R_o = 10^{-3}$, $R_a = 500$, $q = 1$ (regime II). These regimes were obtained after some preliminary calculations in the length of about one diffusion time. We see that in both cases the magnetic energy is larger than the kinetic energy (3 times in case I and 12 times in case II) and the magnetic field has a substantial influence on the flow. If it were not so, the exponential behavior of the magnetic field would happen over such a time interval. The backward influence of the magnetic field on the flow can be estimated by comparison of the kinetic energies with and without the magnetic field. In both cases the ratios of the kinetic energies without magnetic field to

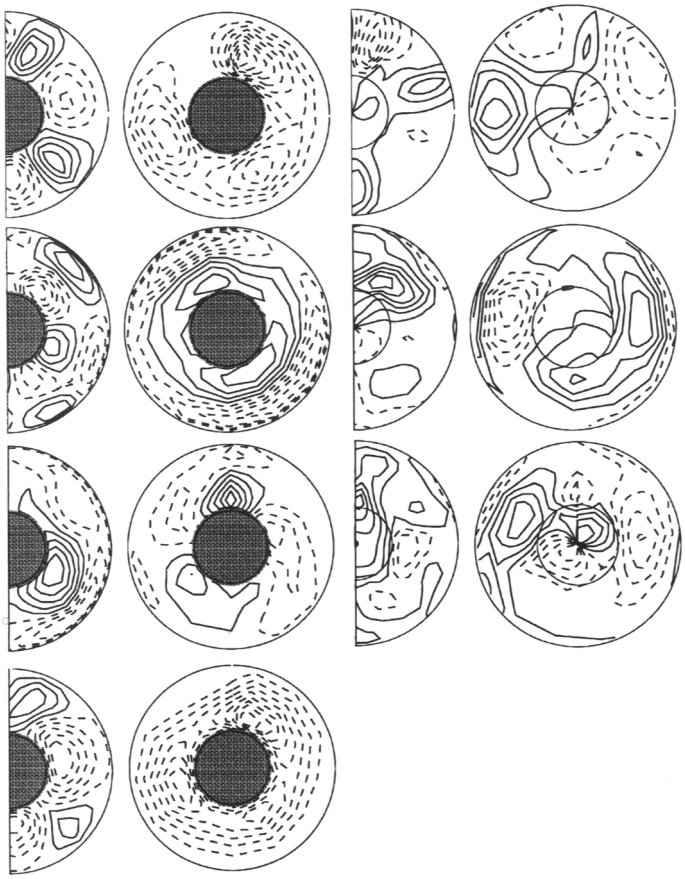

Fig. 3. Case I. The snapshots of the velocity field components (from top to bottom) V_r, V_θ, V_φ and T - two left columns (meridional and equatorial sections) and of the magnetic field - two right columns. The contour lines are equidistantly distributed in ranges (from top to bottom, then from left to right): (–61,51), (–69,44), (–31,52), (–0.5,0.4); (–55,0.7), (–45,43), (–26,43), (–0.7,0.0); (–18,13), (–7,21), (–6,14); (–17,27), (–16,14), (–11,11).

the regime with magnetic field are: 1.4 (case I) and 1.7 (case II). We see, that the large increase of the magnetic energy does not mean a large change in the kinetic energy of the system.

To consider the role of the Lorentz force in more detail, we estimated the ratio of the work of Archimedean and Lorentz forces: $W_{A,L} = \int \left(\boldsymbol{F_{A,L}} \cdot \boldsymbol{V} \right) d\boldsymbol{r}^3$. In both cases the mean value of this ratio was $W_A / W_L \approx 1$. We further calculated quantities $\overline{W_{A,L}} = \int \left| \left(\boldsymbol{F_{A,L}} \cdot \boldsymbol{V} \right) \right| d\boldsymbol{r}^3$ and compared them with the previous ones. The results was

that the Archimedean term stayed nearly unchanged whereas the ratio $W_L / \overline{W_L} \approx 0.3$. It means that the Archimedean force has a larger scale than the Lorentz force and is better correlated with the velocity field.

Another characteristic to be discussed is the angular velocity of the inner core ω. In both cases we can see that the mean level of ω is positive which corresponds to the eastward direction of propagation, if the Earth is considered (*Glatzmaier and Roberts, 1995a,b*). The difference in these regimes is that an increase in the rotation (smaller E)

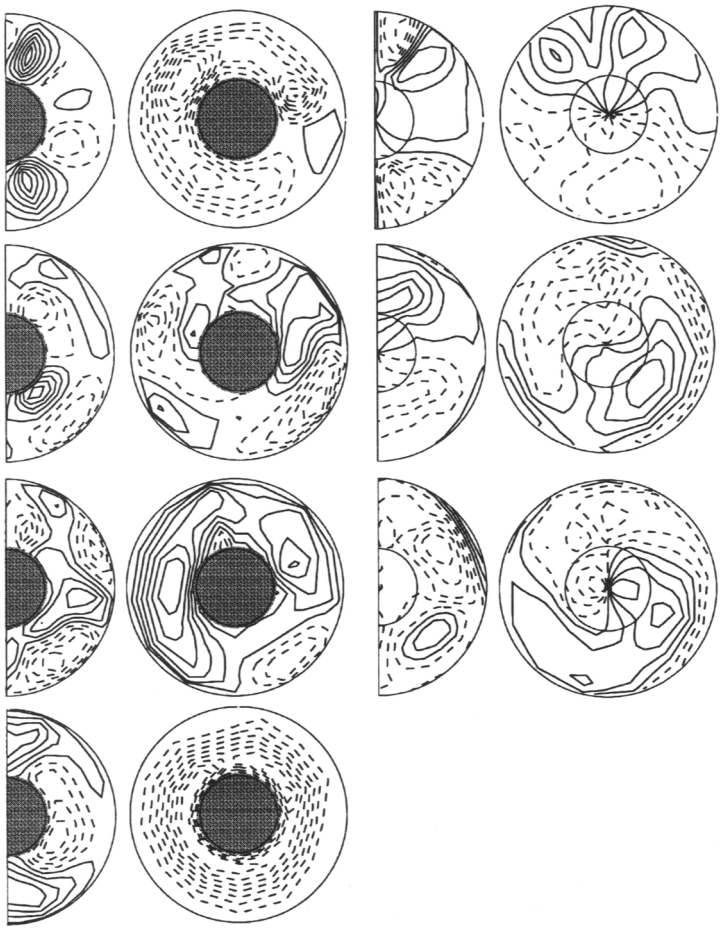

Fig. 4. Case II. The snapshots of the velocity field components (from top to bottom) V_r, V_θ, V_φ and T - two left columns (meridional and equatorial sections) and of the magnetic field - two right columns. The contour lines are equidistantly distributed in ranges (from top to bottom, then from left to right): (–23,60), (–42,61), (–19,19),(–0.6,0.6); (–27,4), (–18,17), (–11,36), (–0.8,0.0); (–4.4, 4.5), (–5.2,7.3), (–3.5,2.6); (–3.1, 3.6), (–1.8,1.5), (–2.7,2.7).

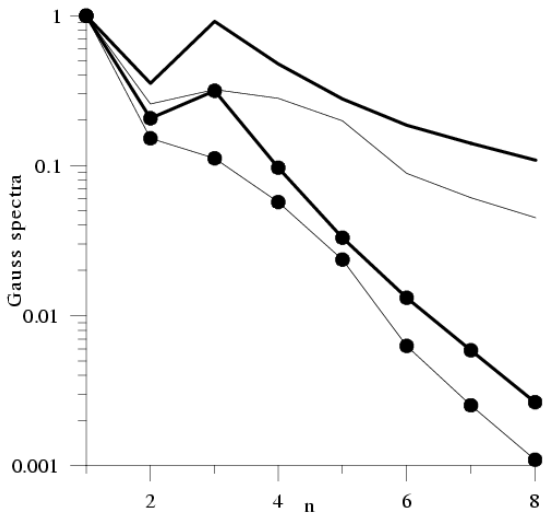

Fig. 5. Gauss spectra of the magnetic field at the CMB and the Earth's surface ($r = 1.7$) (circles) for case I (thin line) and case II (thick) line.

leads to an increase in ω. The reason why the preferable direction of the inner core rotation is eastward follows from the analysis of the flow maps in Figs. 3–4. The difference between the two considered cases can be seen in the plots of the temperature of the meridioanal sections (left, down plots). For case II we observe the well developed temperature structures above (below) the inner core in the tangential cylinder, cf. (*Glatzmaier and Roberts, 1995b*). As it is known (*Aurnou et al., 1996*, see also *Jones, 2000*), the large gradients in these regions lead to the strong thermal wind:

$$\frac{\partial V_\varphi}{\partial z} = \frac{qR_a}{r}\frac{\partial T}{\partial \theta}, \tag{4.2}$$

which causes the viscous torque at the inner core surface.

Our model demonstrates some reversals of the magnetic field. The corresponding behavior of the normalized Gauss coefficients is presented in Fig. 2. We see, that an increase in rotation leads to the state with non-zero mean level of g_1^0. This situation is well known in geomagnetism. Note that similar results were obtained in $\alpha\omega$-modeling when at a bifurcation point the oscillations of about a zero time-average changed with the increase of the dynamo number into vascillations (*Anufriev and Hejda, 1998a*). We also present the Gauss spectra for these two regimes Fig. 5. Both regimes demonstrate a dominant dipole field at the outer core surface and a good convergence for the higher n: the drop of energy is three orders of magnitude. The spectra at the surface $r = 1.7$ (similar to that of the Earth) also decrease by one order of magnitude for the higher n.

5. CONCLUSIONS

We presented the thermal-driven dynamo model based on the full grid approximation in terms of the physical variables, which does not use any filtering in the vicinity of the poles. This model provides a self-consistent magnetic field generation with magnetic energies that are more than one order of magnitude larger than kinetic energy. Although the parameter range was limited by the computer facilities, some qualitative geophysical features were simulated: the dominance of the magnetic field energy over kinetic energy, the eastward direction of the inner core rotation, the dipole structure of the magnetic field and its reversals.

This work is the first step in the development of a grid method based on control volume approach. The hitherto obtained results show that this approach is promising and deserves further elaboration. Our attention will be focused on the problem of numerical stability. Any progress in this direction allows enlarging the scope of parameters or speeding up the integration by lengthening the time step. It is evident that PC is not an adequate tool for the solution of a dynamo problem. We will therefore develop a parallel version of the computer code for PC-clusters or high performance computers.

Acknowledgments: M.R. would like to thank V. Artemeov for a fruitful discussions on numerics. Authors are grateful to the Research Computing Center of Moscow State University for the computing time provided. This work was supported by INTAS foundation (grant 99-00348), the Russian Foundation of Basic Research (grant 00-05-65258) and by the Grant Agency of the Academy of Sciences of the Czech Republic (grant A3012006).

References

Anufriev A.P., Cupal I. and Hejda P., 1995. The weak Taylor state in $\alpha\omega$-dynamo. *Geophys. Astrophys. Fluid. Dynam.*, **79**, 125–145.

Anufriev A.P. and Hejda P., 1998a. Effect of the magneic field at the inner core boundary on the flow in the Earth's core. *Phys. Earth Planet. Inter.*, **106**, 19–30.

Anufriev A.P. and Hejda P., 1998b. The influence of a homogeneous magnetic field on the Ekman and Stewartson layers. Stud. Geophys. Geod., **42**, 254–260.

Aurnou J.M., Brito D. and Olson P.L., 1996. Mechanics of inner core super-rotation. *Geophys., Res.*, **23**, 3401–3407.

Braginsky S.I., 1976. On nearly axially-symmetrical model of the hydromagnetic dynamo of the Earth. *Phys. Earth Planet. Inter.*, **11**, 191–199.

Braginsky S.I. and Roberts P.H., 1987. A model-Z geodynamo. *Geophys. Astrophys. Fluid. Dynam.*, **38**, 327–349.

Christensen U.R., Aubert J., Cardin P., Dormy E., Gibbons S., Glatzmaier G.A., Grote E., Honkura Y., Jones C., Kono M., Matsushima M., Sakuraba A., Takahashi F., Tilgner A., Wicht J., and Zhang K., 2001. A numerical dynamo benchmark. *Phys. Earth Planet. Inter.* **128**, 25–34.

Evans C.R. and Hawley J.F., 1988. Simulation of hydrodynamic flows: A constrained transport method. *Astrophys. J.*, **332**, 659–677.

Fletcher C.A., 1988. *Computational Techniques for Fluid Dynamics*. Springer-Verlag, Berlin.

Gilman P.A. and Miller J., 1981. Dynamical consistent nonlinear dynamos dryven by convection in a rotating shell. *Astrophys. J. Suppl.*, **46**, 211–238.

Glatzmaier G.A. and Roberts P.H., 1995a. A three-dimension self-consistent computer simulation of a geomagnetic field reversal. *Nature*, **377**, 203–209.

Glatzmaier G.A. and Roberts P.H., 1995b. A three-dimension convective dynamo solution with rotating and finitely conducting inner core and mantle. *Phys. Earth Planet. Inter.*, **91**, 63–75.

Glatzmaier G.A. and Roberts P.H., 1996. An anelastic evolutionary geodynamo simulation driven by compositional and thermal convection. *Physica D*, **97**, 81–94.

Hejda P. and Reshetnyak M., 2000. The grid-spectral approach to 3-D geodynamo modelling. *Computers and Geosciences*, **26**, 167–175.

Hejda P., Cupal I. and Reshetnyak M., 2001. On the application of grid-spectral method to the solution of geodynamo eqution. In: P. Chossat, D. Armbruster and I. Oprea (Eds.), *Dynamo and Dynamics, a Mathematical Challenge*, *Nato Sci. Ser.*, **II/26**, Kluwer Acad. Publ., 181–187.

Jones C.A., 2000. Convection-driven geodynamo models. *Phil.Trans. R. Soc.*, **A358**, 873–897.

Kageyama A., Watanabe K. and Sato T., 1993. Simulation study of a magnetohydrodynamic dynamo: Convection in a rotating spherical shell. *Phys. Fluids*, **B5**, 2793–2805.

Kuang W. and Bloxham J., 1997. An Earth-like numerical dynamo model. *Nature*, **389**, 371–374.

Nakajima T. and Roberts P.H., 1995. An application of mapping method to asymmetric kinematic dynamos. *Phys. Earth Planet. Inter.,* **91**, 53–61.

Patankar S.V., 1980. *Numerical Heat Transfer And Fluid Flow*. Taylor and Francis, Philadelphia, London.

Roberts P.H., 1968. On the thermal instability of a rotating-fluid sphere containing heat sources. *Phil. Trans. R. Soc.*, **A263**, 93–117.

Tilgner A. and Busse F.H., 1997. Finite amplitude in rotating spherical fluid shells. *J. Fluid. Mech.*, **332**, 359–376.